Ultrafast and Anisotropic Vibrational Energy Transfer in a β-Barrel Heme Protein: Orientation Dependence in a Cylindrical Protein Matrix

Satoshi Yamashita, Misao Mizuno,[†] Haruto Ishikawa and Yasuhisa Mizutani[*]

Department of Chemistry, Graduate School of Science, The University of Osaka, 1-1 Machikaneyama, Toyonaka, Osaka 560-0043, Japan.

Corresponding Author

Yasuhisa Mizutani — *Department of Chemistry, Graduate School of Science, The University of Osaka, 1-1 Machikaneyama, Toyonaka, Osaka 560-0043, Japan*; orcid.org/ 0000-0002-3754-5720; Email: mztn@chem.sci.osaka-u.ac.jp; Phone: +81-6-6850-5776.

Present Address

[†]Department of Chemistry, Graduate School of Science, Kyoto University, Kitashirakawa-Oiwakecho, Sakyo-ku, Kyoto 606-8502, Japan.

ABSTRACT

Vibrational energy exchange is a fundamental process that governs how proteins overcome energy barriers during their function, and heme proteins are excellent model systems for its investigation. The migration of excess energy released by the heme prosthetic group can be directly monitored using time-resolved anti-Stokes ultraviolet resonance Raman spectroscopy. Crucially, the anti-Stokes Raman intensity from a tryptophan residue acts as an exquisite probe for this excess energy, enabling its location to be mapped with single amino acid spatial resolution. Here, we investigated the dependence of vibrational energy transfer on the orientation of the heme and tryptophan residue within nitrobindin from *Arabidopsis thaliana*, a β-barrel protein containing a heme group. Tryptophan residues were systematically introduced into the protein's cylindrical structure to sample the excess energy in the heme's vicinity for different spatial orientations of the residues. By combining time-resolved anti-Stokes ultraviolet and visible resonance Raman spectroscopy—selectively probe tryptophan residues and the heme group, respectively—we revealed that the vibrational energy transfer from the heme group to its immediate surroundings in nitrobindin is ultrafast and orientationally anisotropic, where atomic contacts within the protein play a critical role.

I. INTRODUCTION

The rate of a chemical reaction is fundamentally determined by the frequency with which a nuclear motion, which transitions reactants to products, acquires the sufficient energy needed to surmount the activation barrier.[1-3] In condensed phases, such as solutions, this necessary energy is supplied to the reactive mode via both intramolecular and intermolecular energy transfer. A critical factor is the relative rate of this energy supply to the reactive mode compared to its dissipation into the solvent and unreactive solute modes, which ultimately governs the reaction's rates, pathways, and efficiency. Therefore, vibrational dynamics serve as the underlying mechanism for the chemical evolution of a molecule.

Time-resolved vibrational spectroscopy has been the primary tool for widely studying intermolecular vibrational energy transfer in solutions.[4-14] The technique works by injecting excess vibrational energy into solute molecules using an ultrashort laser pulse, then tracking the energy's path by observing the population decay of the excited solute modes and the corresponding energy buildup in the solvent. This relaxation process, which sees energy flow from the solute into the solvent's degrees of freedom, occurs rapidly on the 1 to 100 picosecond timescale.[15-17] Despite extensive experimental focus on solutions, the constant, random motion of molecules in a liquid makes it impractical to investigate the orientation dependence of vibrational energy transfer, limiting our mechanistic understanding.

Conversely, the well-defined, unique three-dimensional structures of proteins offer an ideal platform for studying intermolecular vibrational energy transfer, specifically because they enable measurements that are otherwise impossible in solution.[18-23] Heme proteins are particularly well-suited for this research because the photoexcited heme group undergoes ultrafast internal conversion (within 100 fs), returning to the electronic ground state.[24, 25] This process locally

deposits a large amount of excess vibrational energy (as high as 25,000 cm^{-1}) at the heme site immediately after photoexcitation via the B (Soret) transition. Consequently, the heme group acts as a highly efficient photothermal energy converter and local heater.[26, 27] Indeed, we previously showed that this excess energy is rapidly released from the heme site within 1–2 ps.[28, 29] The energy transferred from the heme then flows into the protein moiety before finally dissipating into the surrounding solvent water over a few tens of picoseconds. We exploited the protein's structural stability to investigate distance dependence directly: specifically, we measured energy transfer across varying heme-tryptophan distances that were spaced with the predictable, quasi-constant length of α-helices in cytochrome b_{562}.[30] Beyond mere transfer mechanics, vibrational energy transfer is fundamentally important to understanding protein reactions. These reactions are confined to specific active sites, and the surrounding protein matrix is the necessary medium. Consequently, a core challenge in protein biophysics is understanding precisely how the protein matrix either dissipates reaction-generated energy or transports energy to activate the active site.

The anti-Stokes intensity of a Raman band originates exclusively from vibrationally excited states, making it a highly selective probe for monitoring vibrationally excited populations. We have specifically developed time-resolved anti-Stokes ultraviolet resonance Raman (UVRR) spectroscopy to study vibrational energy flow in proteins.[26, 30-36] This technique is powerful because excitation in the 210–250 nm range resonantly enhances the Raman scattering of aromatic amino acid residues, notably tryptophan (Trp), tyrosine (Tyr), and phenylalanine (Phe).[37-41] This resonance allows us to measure the amount of excess vibrational energy in proteins with the exceptional spatial resolution of a single amino acid residue. These distinct advantages establish time-resolved anti-Stokes UVRR spectroscopy as a robust and essential tool for investigating dynamic vibrational energy transfer within complex protein environments.

In the present study, we utilized nitrobindin to investigate the orientation dependence of vibrational energy transfer within the protein. Figure 1 displays the X-ray crystal structure of *Arabidopsis thaliana* nitrobindin (PDB ID: 3emm).[42] This protein adopts a β-barrel structural motif, composed of 166 amino acids forming ten antiparallel β-strands and containing a heme prosthetic group. We leveraged the protein's cylindrical structure to systematically position a probe residue to sample the excess energy in the vicinity of the heme from different orientations. Three nitrobindin mutants were prepared, each incorporating a single Trp probe residue at a distinct position (46, 76, and 159) in the heme vicinity. A comparison of the spectroscopic data from these mutants allowed direct assessment of the orientation dependence of the heme–Trp vibrational energy transfer. This was possible because the two intrinsic Trp residues in wild-type (WT) nitrobindin are too far from the heme to contribute to the observed anti-Stokes signals. The combination of time-resolved anti-Stokes UVRR spectroscopy (monitoring the Trp residue) and time-resolved anti-Stokes visible resonance Raman (RR) spectroscopy (monitoring the heme) revealed that the vibrational energy transfer to the residues in heme's vicinity in nitrobindin is both ultrafast and anisotropic.

II. EXPERIMENT

A. Sample Preparation

The gene encoding WT nitrobindin from *Arabidopsis thaliana* was codon-optimized for expression in *Escherichia coli* based on the amino acid sequence reported by Bianchetti et al.[42] The gene was subsequently cloned into the pET-17b expression vector by GenScript Japan, which results in the addition of an N-terminal 6×His-tag. For mutagenesis, the PrimeSTAR MAX DNA Polymerase site-directed mutagenesis method (Takara Bio, Japan) was employed according to a standard protocol. The primer sequences used for mutagenesis are listed in Table S1.

Escherichia coli cells harboring the plasmid encoding nitrobindin were cultured at 37 °C in 2×YT or Plusgrow II medium (Nacalai Tesque, Japan) supplemented with 50 μg/mL ampicillin. Expression of the N-terminal 6×His-tagged protein was induced by adding 1 mM isopropyl β-D-thiogalactopyranoside (IPTG) at 37 °C for overnight. The harvested cells were suspended in a buffer consisting of 50 mM Tris-HCl (pH 8.0), 50 mM NaCl, and 2 mM EDTA, and subsequently lysed by sonication using an ultrasonic homogenizer (VP-30S, TAITEC, Japan). The resulting suspension was centrifuged (CF15RXII, Hitachi, Japan) to separate the supernatant from the membrane fragments. Proteins were purified using nickel-Sepharose affinity chromatography (HisTrap HP, GE Healthcare). Following loading onto the column, non-specifically bound proteins were removed by extensive washing with 50 mM Tris-HCl buffer (pH 7.5) containing 50 mM imidazole. The His-tagged nitrobindin was then eluted with a linear gradient of mixing the wash buffer and 50 mM Tris-HCl buffer (pH 7.5) containing 1 M imidazole. The fractions containing purified nitrobindin were dialyzed against 50 mM Tris-HCl buffer (pH 8.0) at 4 °C. Heme incorporation was achieved by adding hemin, dissolved in dimethyl sulfoxide, to a final concentration of 500 mM, followed by centrifugation to remove any precipitated hemin. The purity of the nitrobindin samples was confirmed using SDS-PAGE analysis.

B. Time-Resolved UVRR Measurements

Picosecond pulses at 800 nm were generated by a mode-locked Ti:sapphire oscillator (Tsunami, Spectra-Physics) with a pulse width of approximately 100 fs and a repetition rate of 82 MHz, which was pumped by a diode-pumped solid-state laser (Millennia eV, Spectra-Physics). The seed pulses were amplified by a picosecond-Ti:sapphire regenerative amplifier (Spitfire, Ace MKS Spectra-Physics) pumped by a diode-pumped solid-state, Q-switched laser (Ascend, MKS Spectra-Physics) with a wavelength of 527 nm operated at 1 kHz. The width of the amplified 800 nm pulse

was approximately 1.5 ps. The output pulse with an energy of 4 mJ was divided into halves to generate the pump and probe pulses. One half of the output was converted to 400 nm pulse using the second harmonic generation with an LBO crystal. The other half was introduced into an automated optical parametric amplifier (TOPAS-P, Light Conversion) to obtain 466 nm pulse, which was frequency-doubled using a BBO crystal to generate 233 nm pulse. The components other than 233 nm light were removed spatially with a Pellin-Broca prism and spectrally with an etalon. The 400 and 233 nm pulses were used as pump and probe pulses, respectively. A computer-controlled single-axis optical stage was equipped in the pump arm to adjust the timing between the pump and probe pulses. After the pump and probe pulses were made coaxial using a dichroic mirror, the pump and probe pulses were focused with a cylindrical lens onto a flowing thin film of sample solution formed by a wire-guided jet nozzle. The energies of the pump and probe pulses at the sample position were 20 and 1.0 μJ, respectively. The Raman scattered light was introduced into a Czerny-Turner configured quartz Littrow prism prefilter coupled to a single spectrograph (500M, Spex). The dispersed light in the spectrograph was detected with a liquid-nitrogen-cooled charge-coupled device (CCD) camera (SPEC-10:400B/LN, Roper Scientific). The spectrograph was calibrated using Raman bands of cyclohexane, 2-propanol, and aqueous solution of L-Trp. The cross-correlation width between the pump and probe pulses was determined to be 3.4 ps by measuring intensity of the sum frequency generation of the pump and probe pulses with a thin BBO crystal. The sample solution was replaced with fresh solution every 90 min during time-resolved UVRR measurements. The UVRR measurements were conducted at room temperature. The protein concentration of the sample was 50 μM. Sodium sulfate was added to the sample solution as an internal Raman intensity standard to normalize the intensity changes caused by laser drift and the self-absorption effect.

C. Time-Resolved Visible RR Measurements

The output of the laser system described in the previous section was divided into halves and separately introduced into the automated optical parametric amplifier to generate the pump and probe pulses of 534 and 442 nm, respectively. After the pump and probe pulses were made coaxial using a dichroic mirror, the pump and probe pulses were focused with a cylindrical lens onto sample solution contained in a ⌀10 NMR tube and spun with a spinning cell device. The energies of the pump and probe pulses at the sample position were 20 and 1.0 μJ, respectively. The Raman scattered light was introduced into a Czerny-Turner configured BK7 Littrow prism prefilter coupled to a single spectrograph (500M, Spex). The dispersed light in the spectrograph was detected with a liquid-nitrogen-cooled CCD camera (SPEC-10:400B/LN, Roper Scientific). The spectrograph was calibrated using Raman bands of cyclohexane, acetone, and 2-propanol. The cross-correlation width between the pump and probe pulses was determined to be 2.1 ps by measuring intensity of the sum frequency generation of the pump and probe pulses with a thin BBO crystal. The sample solution was replaced with fresh solution every 60 min during time-resolved visible RR measurements. The visible RR measurements were conducted at room temperature. Sodium sulfate was added to the sample solution as an internal Raman intensity standard to normalize the intensity changes caused by laser drift and the self-absorption effect.

III. RESULTS AND DISCUSSION

Figure 2 shows the time-resolved anti-Stokes UVRR spectra of nitrobindin mutants, Y46W, H76W, and L159W, upon the photoexcitation of heme. In these mutants, an amino acid residue locating near the heme group was replaced with a Trp residue (Fig. 1). The top traces of each panel are the steady-state anti-Stokes UVRR spectra of the mutants, measured only with irradiation of the probe pulse without photoexcitation of heme. For all mutants, the observed bands were

attributed to Trp residue(s) based on UVRR spectra reported for aqueous Trp solutions.[37] The bands observed at 1010, 873, and 761 cm^{-1} were assigned to the out-of-phase indole ring breathing (W16), benzene ring deformation and in-plane NH bending (W17), and in-phase indole ring breathing (W18) modes of Trp, respectively.[37] The Trp vibrational modes W16, W17, and W18 follow the nomenclature established in the vibrational assignment study by Harada and Takeuchi.[37] The asterisk marks the band of the totally symmetric mode of sulfate ion dissolved in the sample solutions for internal intensity standard. The intensities of the anti-Stokes bands in the steady-state spectra arose from the contribution of the vibrationally excited populations at the equilibrium at room temperature.

Other traces in each panel of Fig. 2 are the time-resolved difference spectra for each mutant from −5 to 50 ps. The difference spectra were obtained by subtracting the steady-state spectra from the time-resolved spectra at each delay time probed after photoexcitation of heme by pump pulses. Subtraction was performed after intensity correction for the self-absorption effect and drift in laser power, based on the intensity standard of the sulfate band. The positive anti-Stokes UVRR bands for the W18 mode appeared in the difference spectra at positive delay times.

WT nitrobindin has two Trp residues, Trp30 and Trp67.[42] The distances from heme to Trp30 and Trp67 are 21.8 and 15.1 Å, respectively. These distances were determined as the distance from the iron atom of the heme molecule and the center of mass of the indole ring of each Trp residue. The top traces in Fig. 2 contain the contributions of all Trp residues in the proteins, thus, the native Trp residues can contribute to the band intensities in the time-resolved difference spectra in addition to the introduced Trp residue. However, in our previous work using myoglobin mutants, a probe Trp residue which is located at the position more distant than 15.0 Å did not contribute to spectral changes in anti-Stokes UVRR spectra.[32] This suggests that the contributions of Trp30 and

Trp67 to the spectral changes in the anti-Stokes UVRR spectra were negligible. To examine the contributions of two native Trp residues to the band intensities in the time-resolved spectra, we measured time-resolved anti-Stokes UV resonance Raman spectra of WT nitrobindin upon the photoexcitation of heme. No bands were observed in the time-resolved difference spectra for WT nitrobindin (see Fig. S1), meaning that the contributions of Trp30 and Trp67 to the spectral changes in the anti-Stokes UVRR spectra were negligible. These results demonstrated that the band intensities observed in the time-resolved anti-Stokes UVRR difference spectra of the nitrobindin mutants were attributed to the introduced Trp residue.

The intensity changes of the anti-Stokes UVRR band arise from the changes of populations in the vibrationally excited states and/or those of the UVRR cross-sections for the given vibrational modes. The UVRR cross-section depends on the Trp residue's environment and side-chain conformation. If the anti-Stokes intensity changes resulted from cross-section alternations, the Stokes UVRR bands in the time-resolved difference spectra should exhibit changes comparable to the anti-Stokes bands. However, our measurements of time-resolved Stokes UVRR spectra for nitrobindin (Fig. S2) revealed that the intensity changes of the Stokes bands were considerably smaller than those of anti-Stokes bands. Hence, the contribution of the changes of the cross-section is negligible, and the intensity changes of anti-Stokes Trp bands directly show the population changes of the vibrationally excited states of the Trp residues.

The observed temporal changes of anti-Stokes UVRR bands show that the Trp residues were vibrationally excited after photoexcitation of heme. We compared temporal changes of the time-resolved anti-Stokes UVRR intensities of the Trp46, Trp76, and Trp159 in three mutants. Figure 3 shows the temporal intensity changes of anti-Stokes W18 bands in time-resolved difference spectra of the nitrobindin mutants. The anti-Stokes intensities, which were calculated as the area

intensity, are shown as the relative intensities of the pump-induced intensity differences of the W18 band to the W18 band intensity in the steady-state spectrum. The rise and decay are due to vibrational excitation due to the energy released by heme and subsequent vibrational relaxation in the Trp residue. It is intriguing that the W18 intensity rise for H76W and L159W mutants were nearly instantaneous, which was never observed in previous studies on various heme proteins,[30-33, 35] suggesting ultrafast energy transfer from the heme group. In contrast, the anti-Stokes intensity of the Y46W mutant is systematically shifted toward later delay times compared to those of the H76W and L159W mutants, suggesting a slower rise in intensity.

We analyzed the temporal evolutions of the anti-Stokes UVRR intensities for the mutants to determine the rate of intensity rise and decay. The temporal changes were fitted with a biexponential function convoluted with the instrumental response function. The results of the fitting are indicated by solid lines in Fig. 3. The obtained time constants of the rise of the W18 bands were 3.2±1.1, 0.5±0.2, and 0.9±0.3 ps for Y46W, H76W, and L159W, respectively. The time constants of the decay were 9.7±1.7, 8.9±0.9, and 8.5±0.9 ps for Y46W, H76W, and L159W, respectively.

No significant difference was observed in the decay time constant among the three mutants, but a pronounced difference was detected in the rise time constant. To investigate whether the ultrafast vibrational excitation for H76W and L159W mutants is due to ultrafast energy relaxation of the heme group in these mutants and whether the difference in the W18 rise of Y46W mutant from those of the other two mutants stemmed from anisotropy in heme energy relaxation, we measured the time-resolved anti-Stokes visible RR spectra of the heme group in the mutants. Figure 4 illustrates the temporal intensity changes of the anti-Stokes ν_4 (pyrrole half-ring symmetric stretching) bands of heme derived from the time-resolved difference visible RR spectra of WT

nitrobindin and the nitrobindin mutants (Fig. S3). These temporal changes indicate that the rates of vibrational relaxation of heme were similar across WT and the three nitrobindin mutants and comparable to myoglobin[28, 29] and cytochrome *c*.[31] These results exclude the possibility that the observed difference in the vibrational excitation for H76W and L159W mutants is due to a difference in vibrational energy relaxation of the heme group in these mutants and suggest orientational anisotropy in the rate of energy transfer from the heme group to the Trp residue.

It is intriguing that the vibrational excitation of the Trp residues is faster than the heme relaxation in H76W and L159W mutants, which raises two potential explanations for the observed difference in the rise time constant: (i) the Trp side chain is electronically excited simultaneously with the heme group by the pump pulse due to the Trp–heme overlap of electronic wavefunctions, or (ii) vibrational energy deposited into the heme rapidly are shared with the Trp residues via efficient pathways.

We first assessed possibility (i). B and Q absorption bands of porphyrins exhibited shifts and intensity variations due to electronic interactions.[43-45] If electronic interaction were significant, the UV-vis absorption spectra of H76W and L159W mutants would be perturbed by the nearby Trp residue. However, their absorption spectra were found to be very similar to that of WT nitrobindin and Y46W mutant (Fig. S4). This result suggests that the simultaneous electronic excitation of the heme and the nearby Trp residue is less probable.

Next, we investigated possibility (ii). Structural properties, including the distance between heme and probe residues, solvent accessible surface area, hydrogen bonds, and atomic contacts, are fundamentally related to the mechanism of intramolecular energy flow in proteins.[32, 33, 35] Trp159 is situated in the tenth β-strand, which includes His158 forming the sole covalent linkage to the heme group.[42] In contrast, Trp46 and Trp76 are located in the second and fourth β-strands,

respectively. Consequently, the distances between the heme and each Trp residue when measured along the protein backbone are significantly different. If the excess energy deposited into the heme were to flow to the Trp residues along this main chain, the time constants observed for energy transfer should exhibit a correlation with the distances along the backbone. However, the rise time constant measured for Trp46 was found to be smaller than that for Trp76. This lack of correlation between the rise time constant and the backbone distance strongly suggests that the energy is transferred not via covalent linkages within the protein backbone but primarily through atomic contacts between the heme group and the surrounding residues. This interpretation is further supported by the experimental contrast: while we succeeded in isolating Trp mutants of nitrobindin (comprising ten anti-parallel β-strands), we were unable to obtain similar Trp mutants of nitrophorin 4 (constituted of eight anti-parallel β-strands). This discrepancy suggests that the region surrounding the heme within the β-barrel structure is so tightly packed by surrounding atoms that the introduction of a bulky Trp residue is only tolerated in the more accommodating geometry of the ten-stranded structure.

While the crystal structure of WT nitrobindin is available, those for the nitrobindin mutants investigated in this study have not yet been determined. We calculated the protein structures for Y46W, H76W, and L159W nitrobindin mutants to gain structural insights by the use of homology modeling performed with MODELLER via the UCSF Chimera-accessible web service.[46, 47] The resultant structures for the Y46W, H76W, and L159W mutants are illustrated in Fig. 5A. In all three mutants, the side chain of the probe Trp residue is positioned in close vicinity to the heme group, suggesting the presence of atomic contacts with the heme group. Furthermore, the Trp side chains in H76W and L159W mutants are observed to be stacked parallel to the heme plane, whereas the Trp side chain in Y46W mutant is not. This distinct difference in the stacking

geometry is likely the origin of the ultrafast vibrational energy transfer for H76W and L159W mutants and the observed differences in the rate of the vibrational energy transfer between Y46W mutant and the other two mutants.

Our previous study on myoglobin demonstrated that the primary pathway for vibrational energy transfer from the heme is through atomic contacts.[33, 35] Therefore, an increased extent of atomic contacts should correlate with an increased rate of energy flow into the Trp residue. To quantify and compare the heme–Trp atomic contacts, we calculated the interatomic distances for all atomic pairs between an atom in the heme group and an atom of the probe Trp residue, based on the protein structures predicted by MODELLER. We then counted the number of pairs whose interatomic distance is smaller than a certain threshold value. Figure 5B plots the number of atomic pairs between the heme and each probe Trp residue within the threshold distance. Given the carbon atom radius of 1.7 Å, we examined atom pairs separated by a distance of 4.4 Å or less (twice the radius plus 1.0 Å). A comparison of these numbers reveals that the count for Y46W was significantly smaller than those for the other two mutants (H76W and L159W). Furthermore, the number of pairs for H76W and L159W were relatively similar to each other and larger than the counts previously observed in myoglobin mutants,[33] which is consistent with the ultrafast vibrational excitation for these mutants. This suggests that the substantial extent of atomic contacts between the heme and Trp residue in H76W and L159W creates a highly efficient energy transfer pathway through which the vibrational energy of the heme is very rapidly shared with the Trp residue. High packing would suppress the fluctuation of the distance between the heme and the Trp residue. Stock and Leitner showed that the energy transfer rate scales inversely proportional to the variance in the donor-acceptor distance.[48-52] High packing is also likely to be associated with ultrafast energy transfer due to lower structural fluctuations.

We verified the validity of the kinetic scheme presented in Fig. 6A for modeling the observed intensity changes of the anti-Stokes bands associated with the heme group and the Trp residues. Utilizing this scheme, we calculated the excess energy within the heme group and the probe Trp residue by solving the rate equations (detailed in the Supplementary Material), yielding the temporal profiles shown in Fig. 6B and 6C, respectively. The temporal profiles of the excess energy were simulated for various rates of energy transfer between the heme group and the Trp residue. Critically, the simulated temporal changes of the excess energy successfully reproduced the features of the observed anti-Stokes intensity dynamics. Specifically, the rise of the excess energy in the Trp residue exhibited a significant dependence on the energy transfer rate, whereas the decay in the heme group was less sensitive. These findings strongly support our interpretation that the energy transfer from the heme group to its vicinity is anisotropic and that the transfer to the amino acid residues stacking with the heme group occurs on a subpicosecond timescale.

IV. SUMMARY

In the present study, we systematically investigated the orientation dependence of vibrational energy transfer by strategically repositioning a Trp residue, a key probe for transient excess energy, along the inner surface of the nitrobindin cylindrical scaffold. By utilizing the unique geometry of the ten anti-parallel β-barrel structure, we were able to vary the Trp–heme orientation without significantly changing the heme–Trp distance. We report the first observation of ultrafast (<1 ps) vibrational excitation in the Trp residues in a stacked arrangement with heme immediately following the photoexcitation of the heme group. Critically, we demonstrated that this energy transfer from the heme to its periphery exhibits pronounced anisotropic characteristics. This anisotropy is attributed to the coplanar structures of both the heme and the Trp side chain, coupled with their extensive atomic contacts in H76W and L159W mutants. Collectively, these findings

confirm the viability of the proposed energy transfer scheme and provide unprecedented, critical insight into the initial, ultrafast steps of energy dissipation within the protein matrix, establishing a fundamental principle for energy transduction in this class of biomolecules.

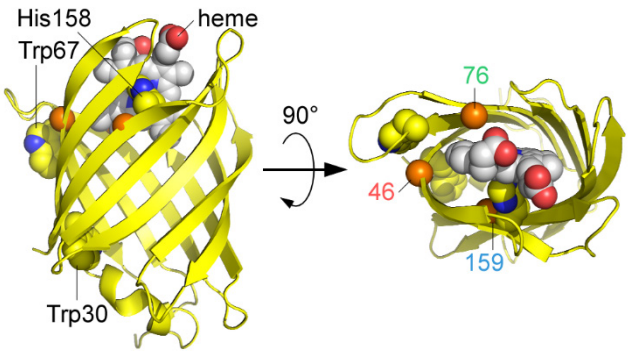

FIG. 1. X-ray crystal structure of WT nitrobindin (PDB ID: 3emm). The protein is shown in yellow ribbon representation. The heme group, the two intrinsic Trp residues (Trp30 and Trp67), and the heme-bound His residue (H158) are rendered as space-filling spheres. The α-carbons of the probe Trp residues engineered at positions 46, 76, and 159 are individually highlighted as space-filling spheres colored orange.

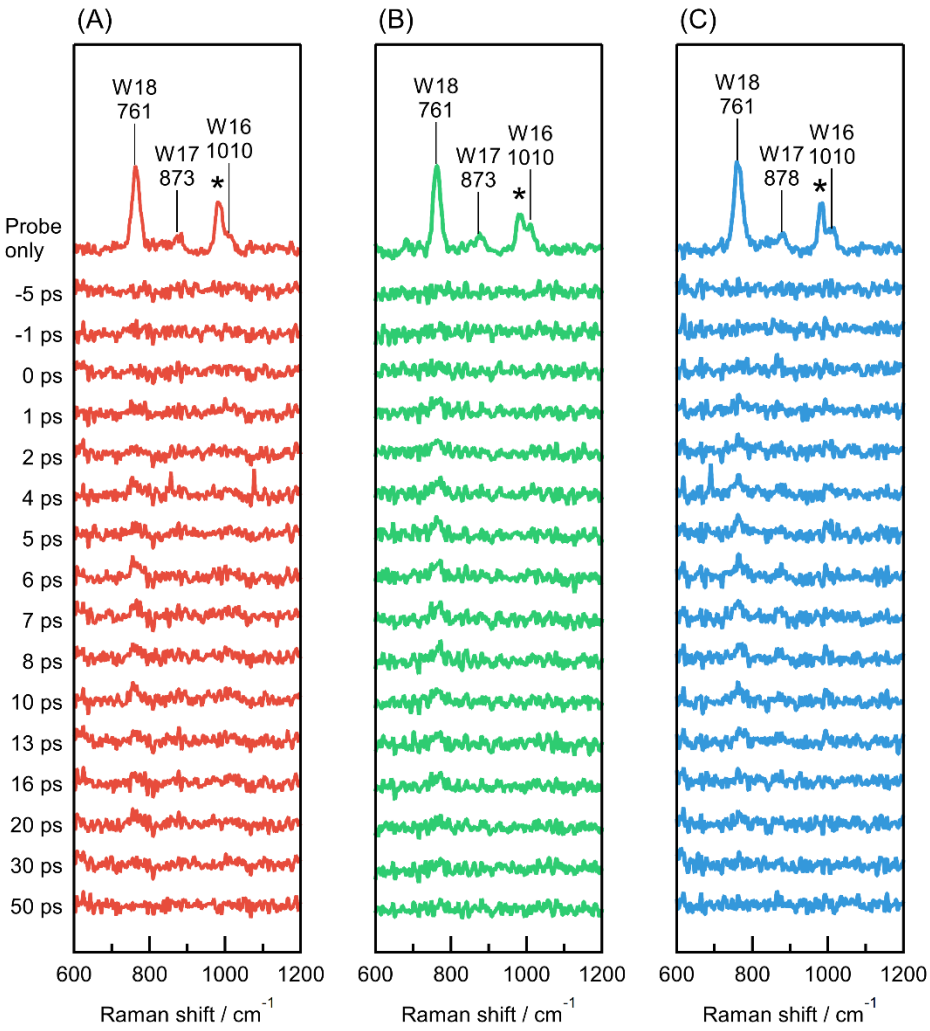

FIG. 2. Time-resolved anti-Stokes UVRR spectra of the nitrobindin mutants. Spectra were probed at 233 nm following 400 nm photoexcitation of the heme group. (A) Y46W, (B) H76W, and (C) L159W mutants are shown. The top traces represent the probe-only anti-Stokes UVRR spectra of the steady states for each mutant. The asterisk (∗) indicates the band attributed to the sulfate ion ($SO4^{2-}$) at 983 cm^{-1}. All other traces show the time-resolved difference spectra, which were obtained by subtracting the probe-only spectrum from the pump-probe spectrum at each delay time. The accumulation time for each spectrum was 90 min.

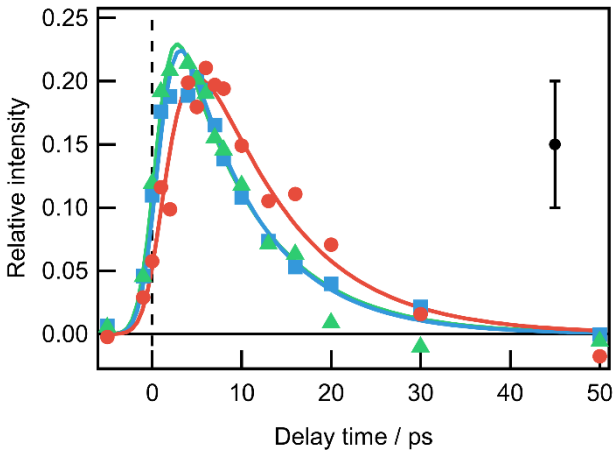

FIG. 3. Temporal profiles of the pump-induced anti-Stokes W18 band intensity of Y46W (red), H76W (green), and L159W (blue) mutants in the range from −5 to 50 ps following photoexcitation. The anti-Stokes intensities are shown as the relative intensities of the pump-induced intensity differences of the W18 band to the W18 band intensity in the steady-state spectrum. Solid lines represent the best fits to a biexponential function convoluted with the instrument response function (IRF). The IRF was approximated by a Gaussian function with a full width at half maximum of 3.4 ps. As indicated by an error bar of black marker in the figure, the typical value of standard deviations of the observed relative intensities was 0.05 for six independent measurements.

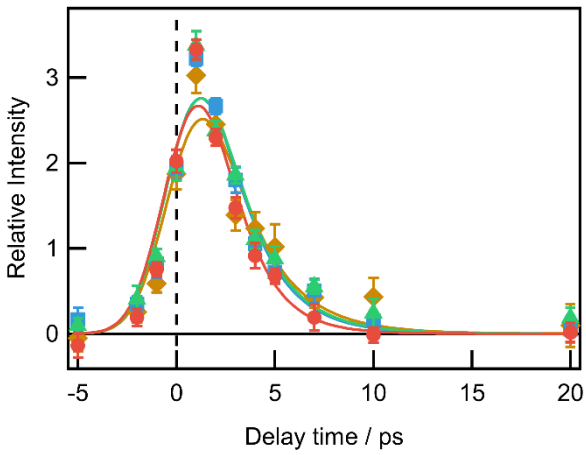

FIG. 4. Temporal profiles of the pump-induced anti-Stokes ν_4 band intensity of WT nitrobindin (brown), Y46W (red), H76W (green), and L159W (blue) mutants in the range from −5 to 20 ps following photoexcitation. Solid lines represent the best fits to a single exponential function convoluted with the IRF, which was approximated by a Gaussian function with a full width at half maximum of 2.1 ps. The error bars represent one standard deviation from the average, which was calculated for four independent measurements.

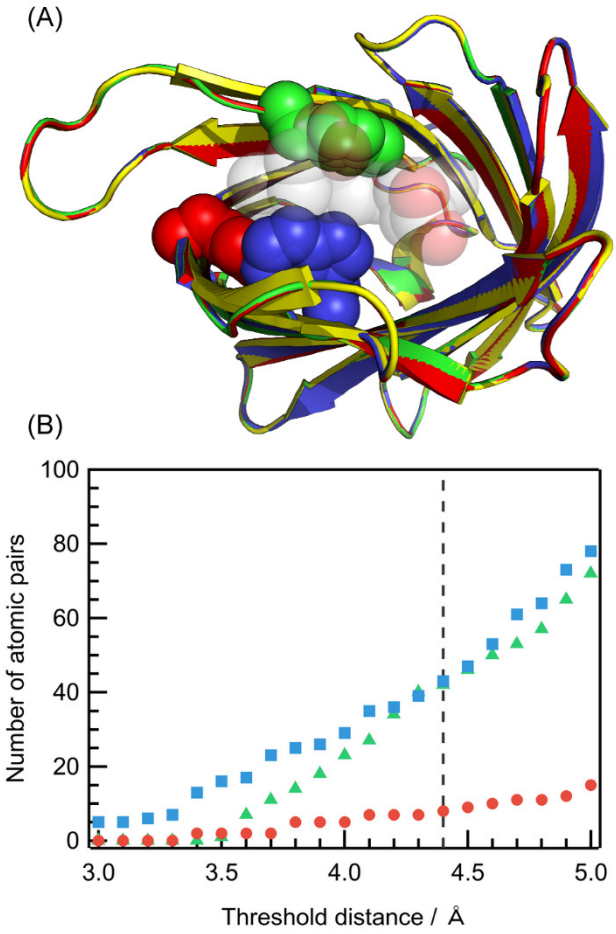

FIG. 5. Atomic contacts of the probe Trp residues to the heme group in nitrobindin. (A) Crystal structure of WT nitrobindin (yellow; PDB ID: 3emm) and predicted protein structures of Y46W (red), H76W (green), and L159W (blue) mutants using MODELLER. The heme group and the probe Trp residues are represented as space-filling spheres. (B) The number of atomic pairs between the heme group and the probe Trp residue plotted against the interatomic distance threshold (Å). Calculations of the number of atomic pairs is described in Fig. S5 in the Supplementary Material. The numbers of atomic pairs are shown in red, green, and blue for Y46W, H76W, and L159W mutants, respectively. The vertical dashed line delineates the threshold value (4.4 Å) used to define contact pairs.

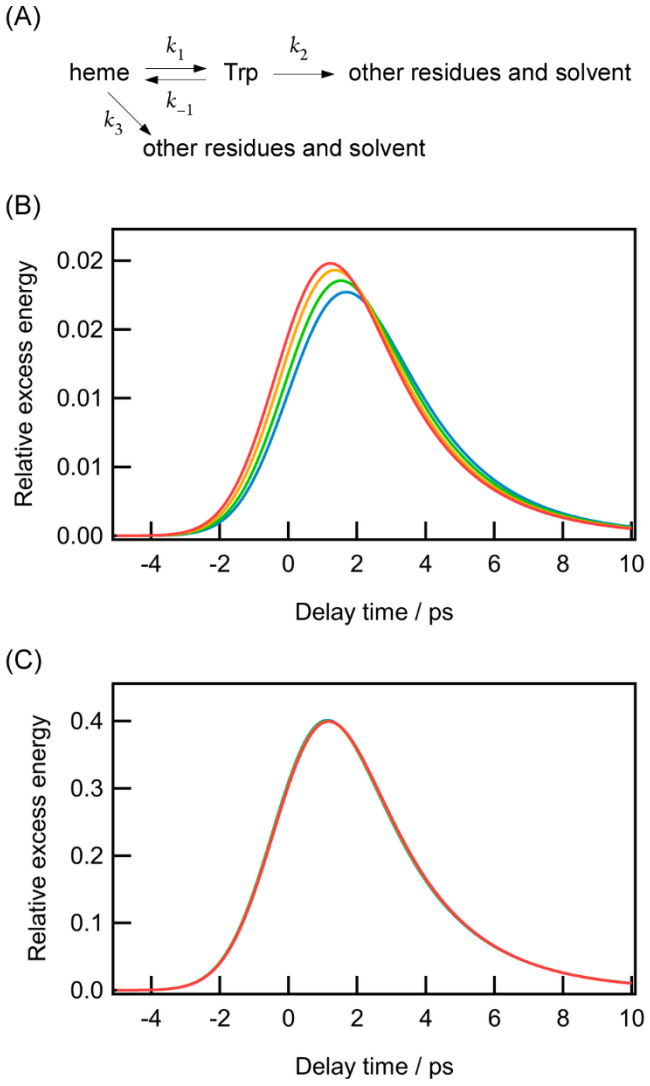

FIG. 6. Kinetic model and simulated temporal profiles for excess energy transfer in nitrobindin. (A) Schematic representation illustrating the excess energy flow deposited in the heme group upon photoexcitation. The temporal profiles are described using four first-order rate constants (k_1, k_{-1}, k_2, and k_3). (B) Simulated temporal profiles of the excess energy in the probe Trp residue. The forward (k_1) and reverse (k_{-1}) rate constants for energy transfer between the heme group and the probe Trp residue are varied: k_1 and k_{-1} are 1/0.5 and 1/0.05 (red), 1/2 and 1/0.2 (orange), 1/4 and 1/0.4 (green), and 1/6 and 1/0.6 ps^{-1} (blue), respectively. The rate constants for energy dissipation to other residues and solvent, k_2 and k_3, are fixed at 1/8 and 1/2 ps^{-1} for all traces. (C) Simulated temporal profiles of the excess energy in the heme group. The rate constant values for each trace are identical to those used in panel B. The analytical solutions to the rate equations based on the scheme in panel A are provided in the Supplementary Material.

Table I. Summary of time constants from anti-Stokes Raman spectroscopy: temporal dynamics of probe Trp residues and heme in nitrobindin.

Protein	Time constants for the probe Trp residue / ps		Time constant for heme / ps
	Rise	Decay	Decay
Y46W	3.2±1.1	9.7±1.7	1.7±0.3
H76W	0.5±0.2	8.9±0.9	2.1±0.3
L159W	0.9±0.3	8.5±0.9	2.0±0.3
WT			2.3±0.4

SUPPLEMENTARY MATERIAL

See the supplementary material for the following: (1) primer sequences used for mutagenesis; (2) time-resolved anti-Stokes UVRR spectra of WT nitrobindin; (3) time-resolved Stokes UVRR spectra of nitrobindin mutants; (4) time-resolved anti-Stokes visible RR spectra of WT nitrobindin and the mutants; (5) UV-vis absorption spectra of WT nitrobindin and the mutants; (6) calculations of numbers of atomic pairs shown in Fig. 5B, and (7) temporal profiles for excess energy transfer in nitrobindin.

ACKNOWLEDGMENTS

This research was supported by the Japan Society for the Promotion of Science through Grant-in-Aid for JSPS Fellows to S.Y. (No. JP19J20486) and Grants-in-Aid for Scientific Research to Y.M. (No. JP17H01184 and JP20H02693) and M.M. (No. JP20H02695), and by the Ministry of Education, Culture, Sports, Science and Technology of Japan through a Grant-in-Aid for Transformative Research Areas (B) "Low-energy manipulation" to M.M. (No. JP20H05756). Molecular graphics and analyses performed with UCSF Chimera, developed by the Resource for Biocomputing, Visualization, and Informatics at the University of California, San Francisco, with support from NIH P41-GM103311.

AUTHOR DECLARATIONS

Conflict of Interest

The authors have no conflicts to disclose.

Author Contributions

Satoshi Yamashita: Data curation (lead); Formal analysis (lead); Investigation (lead); Writing – original draft (equal); Writing – review & editing (equal). **Misao Mizuno**: Investigation

(supporting); Funding acquisition (supporting); Writing – review & editing (equal). **Haruto Ishikawa**: Conceptualization (equal); Investigation (supporting); Writing – review & editing (equal). **Yasuhisa Mizutani**: Conceptualization (equal); Formal analysis (supporting); Supervision (lead); Funding acquisition (lead); Writing – original draft (equal); Writing – review & editing (equal).

DATA AVAILABILITY

The data that support the findings of this study are available from the corresponding author upon reasonable request.

REFERENCES

[1] H. Eyring, J. Chem. Phys. **3** (1935) 107.
[2] M. G. Evans, and M. Polanyi, Trans. Faraday Society **31** (1935) 875.
[3] E. Wigner, J. Chem. Phys. **5** (1937) 720.
[4] J. C. Deàk, L. K. Iwaki, and D. D. Dlott, J. Phys. Chem. A **103** (1999) 971.
[5] L. K. Iwaki *et al.*, Chem. Phys. Lett. **303** (1999) 176.
[6] G. Seifert *et al.*, J. Chem. Phys. **112** (2000) 6349.
[7] Z. Wang, A. Pakoulev, and D. D. Dlott, Science **296** (2002) 2201.
[8] Y. Fang *et al.*, J. Phys. Chem. A **113** (2009) 75.
[9] N.-H. Seong, Y. Fang, and D. D. Dlott, J. Phys. Chem. A **113** (2009) 1445.
[10] H. Bian, W. Zhao, and J. Zheng, J. Chem. Phys. **131** (2009) 124501.
[11] H. Bian *et al.*, J. Chem. Phys. **132** (2010) 184505.
[12] H. Bian *et al.*, J. Chem. Phys. **133** (2010) 034505.
[13] V. Botan *et al.*, Proc. Natl. Acad. Sci. USA **104** (2007) 12749.
[14] I. V. Rubtsov, and A. L. Burin, J. Chem. Phys. **150** (2019) 020901.
[15] T. Elsaesser, and W. Kaiser, Annu. Rev. Phys. Chem. **42** (1991) 83.
[16] A. Seilmeier, and W. Kaiser, in *Ultrashort Laser Pulses*, edited by W. Kaiser (Springer, New York, 1993), p. 279.
[17] J. C. Owrutsky, D. Raftery, and R. M. Hochstrasser, Annu. Rev. Phys. Chem. **45** (1994) 519.
[18] D. M. Leitner, and J. E. Straub, *Proteins: Energy, Heat and Signal Flow* (CRC Press, Boca Raton, FL, 2009),
[19] G. Li, D. Magana, and R. B. Dyer, Nat. Commun. **5** (2014) 3100.
[20] T. Baumann *et al.*, Angew. Chem. Int. Ed. **58** (2019) 2899.
[21] E. Deniz *et al.*, Nat. Commun. **12** (2021) 3284.
[22] J. G. Löffler *et al.*, Angew. Chem. Int. Ed. **61** (2022) e202200648.
[23] C. Feid *et al.*, Angew. Chem. Int. Ed. **63** (2024) e202317047.
[24] P. M. Champion, and R. Lange, J. Chem. Phys. **73** (1980) 5947.
[25] J. W. Petrich, C. Poyart, and J. L. Martin, Biochemistry **27** (1988) 4049.
[26] Y. Mizutani, and M. Mizuno, J. Chem. Phys. **157** (2022) 240901.
[27] T. Watase, M. Mizuno, and Y. Mizutani, J. Phys. Chem. C **129** (2025) 148.
[28] Y. Mizutani, and T. Kitagawa, Science **278** (1997) 443.
[29] Y. Mizutani, and T. Kitagawa, Chem Rec **1** (2001) 258.
[30] S. Yamashita *et al.*, J. Phys. Chem. B **126** (2022) 3283.
[31] N. Fujii, M. Mizuno, and Y. Mizutani, J. Phys. Chem. B **115** (2011) 13057.
[32] N. Fujii *et al.*, J. Phys. Chem. Lett. **5** (2014) 3269.
[33] M. Kondoh, M. Mizuno, and Y. Mizutani, J. Phys. Chem. Lett. **7** (2016) 1950.
[34] Y. Mizutani, Bull. Chem. Soc. Jpn. **90** (2017) 1344.
[35] S. Yamashita *et al.*, J. Phys. Chem. B **122** (2018) 5877.
[36] S. Yamashita, M. Mizuno, and Y. Mizutani, J. Chem. Phys. **156** (2022) 075101.
[37] I. Harada, and H. Takeuchi, in *Advances in Spectroscopy: Spectroscopy of Biological Systems*, edited by R. J. H. Clark, and R. E. Hester (Wiley, New York, 1986), pp. 113.
[38] S. A. Asher, Annu. Rev. Phys. Chem. **39** (1988) 537.
[39] T. Kitagawa, Prog. Biophys. Mol. Biol. **58** (1992) 1.
[40] H. Takeuchi, Biopolymers **72** (2003) 305.
[41] H. Takeuchi, Anal. Sci. **27** (2011) 1077.

[42] C. M. Bianchetti *et al.*, Proteins: Structure, Function, and Bioinformatics **78** (2010) 917.
[43] A. Osuka, and K. Maruyama, J. Am. Chem. Soc. **110** (1988) 4454.
[44] M. Sirish, and H.-J. Schneider, J. Am. Chem. Soc. **122** (2000) 5881.
[45] T. H. Tran-Thi *et al.*, J. Phys. Chem. **96** (1992) 1073.
[46] E. F. Pettersen *et al.*, J. Comput. Chem. **25** (2004) 1605.
[47] Z. Yang *et al.*, J. Struct. Biol. **179** (2012) 269.
[48] S. Buchenberg, D. M. Leitner, and G. Stock, J. Phys. Chem. Lett. **7** (2016) 25.
[49] K. M. Reid, T. Yamato, and D. M. Leitner, J. Phys. Chem. B **122** (2018) 9331.
[50] L. Valiño Borau, A. Gulzar, and G. Stock, J. Chem. Phys. **152** (2020) 045103.
[51] H. Poudel *et al.*, J. Phys. Chem. B **124** (2020) 9852.
[52] K. M. Reid, T. Yamato, and D. M. Leitner, J. Phys. Chem. B **124** (2020) 1148.